Short communication

Sol−gel synthesis and ionic conductivity of oxyapatite-type La$_{9.33+x}$Si$_6$O$_{26+1.5x}$

Wei Liu [a], Shu Yamaguchi [b], Takashi Tsuchiya [c], Shogo Miyoshi [b], Kiyoshi Kobayashi [d], Wei Pan [a,*]

[a] State Key Lab. of New Ceramics and Fine Processing, Department of Materials Science and Engineering, Tsinghua University, Beijing 100084, People's Republic of China
[b] Department of Materials Engineering, The University of Tokyo, 7-3-1 Hongo, Bunkyo, Tokyo 113-8656, Japan
[c] Atomic Electronics Unit, MANA, National Institute for Materials Science, 1-1 Namiki, Tsukuba, Ibaraki 305-0044, Japan
[d] Advanced Materials Processing Unit, National Institute for Materials Science, 1-2-1 Sengen, Tsukuba, Ibaraki 305-0047, Japan

HIGHLIGHTS

▶ Apatite-type La$_{9.33+x}$Si$_6$O$_{26+1.5x}$ are synthesized via a sol−gel process.
▶ Powders with $9.33 + x \leq 10$ calcined at 900 °C are pure oxyapatite phase with grain size of 30 nm
▶ Samples sintered at temperature of 1600 °C have high relative density of more than 95%.
▶ Sintered samples with $9.33 + x \leq 9.5$ are apatite phase.
▶ TheLa$_{9.5}$Si$_6$O$_{26.25}$ exhibits superior ionic conductivity of 1.6×10^{-2} Scm^{-1} at 800 °C.

ARTICLE INFO

ABSTRACT

A series of apatite-type lanthanum silicates La$_{9.33+x}$Si$_6$O$_{26+1.5x}$ (LSO) are synthesized via a sol−gel process. Differential thermal analysis, X-ray diffraction, transmission electron microscopy, scanning electron microscopy and Raman measurements are performed to examine the phase present and morphology of LSO. It revealed that LSOs with $9.33 + x \leq 10$ calcined at 900 °C are identified as pure oxyapatite phase with an average grain size of 30 nm. LSOs with $9.33 + x \leq 9.5$ sintered at 1600 °C are also identified as single apatite phase. Based on 2 and 4-probe AC impedance spectroscopy measurements, the dependence of calcination temperature and composition on the electrical conductivity of LSOs are evaluated. Samples with composition of La$_{9.5}$Si$_6$O$_{26.25}$ and La$_{9.33}$Si$_6$O$_{26}$ function as purely ionic conductors, exhibiting high conductivities of 1.6×10^{-2}S cm^{-1} and 1.3×10^{-2} Scm^{-1} at 800 °C.

© 2013 Elsevier B.V. All rights reserved.

1. Introduction

Solid oxide fuel cells (SOFCs), as a promising environmentally friendly and high efficient energy conversion technology, produce electricity from the electrochemical combination of fuel and oxidant, which attracts considerable attention. Over the years, the development of SOFCs has focused on lowering the operation temperatures to low (300−500 °C) or intermediate (500−700 °C) range, as the elevated operating temperature is the critical technical barrier for commercialization of the SOFCs [1−4]. It is therefore a significant challenge of using materials with high ionic conductivities as solid electrolytes.

In the past score years, as a novel class of oxygen ion conductors, lanthanum silicates La$_{9.33+x}$(SiO$_4$)$_6$O$_{2+1.5x}$ with apatite type structure have developed rapidly due to their higher ionic conductivity than the state-of-the-art yttria-stabilized zirconia (YSZ) at moderate temperatures [4−12]. The ionic conductivities of La$_{9.33}$(SiO$_4$)$_6$O$_2$ are found to be 7.2×10^{-5} Scm^{-1} at 500 °C and 1.4×10^{-3} Scm^{-1} at 800 °C, respectively [9]. In addition, high oxygen ion transference numbers over a wide range of oxygen partial pressures, good mechanical properties and moderate thermal expansion coefficients also facilitate the research of lanthanum silicates as solid electrolytes. Furthermore, compared with most of other ionic conductors, one can find that the apatite-type structure is more tolerant to extensive aliovalent doping, which is an approach to improve oxide ionic conductivity of lanthanum silicates [11].

However, by far the applicability of lanthanum silicates as solid electrolytes is limited due to the high sintering temperature (1700−1800 °C) and extensive holding time for the traditional solid-state reaction [4]. Beside, the easy formation of secondary phases during synthesis, such as La$_2$O$_3$, La$_2$SiO$_5$ or La$_2$Si$_2$O$_7$, is clearly a

* Corresponding author. Tel.: +86 1062772858; fax: +86 1062771160.
E-mail address: panw@mail.tsinghua.edu.cn (W. Pan).

disadvantage in the electrical property of lanthanum silicate [10,11]. Therefore, lots of attention focuses on novel synthesis method to prepare lanthanum silicates of pure oxyapatites at low heat treatment temperature. Only a few researches have been done on the low-temperature sol–gel synthesis [4]. Co-precipitation approaches have also been proposed to prepare the LSO powder [12], whereas impurity still appears and is removed by an extra process of acid-leaching.

In this work, a novel sol–gel synthesis has been used to prepare pure apatite-type $La_{9.33+x}Si_6O_{26+1.5x}$ electrolytes with high sinterability at low formation temperature and superior ionic conductivities.

2. Experimental

Raw materials of lanthanum nitrate hexahydrate (La(NO$_3$)$_3$·6H$_2$O, 3 N, Wako Pure Chemical Industry Inc., Japan), amorphous silicon dioxide (SiO$_2$, 3 N with specific surface area of 200 m^2 g^{-1}, Wako Pure Chemical Industry Inc., Japan) and citric acid (C$_6$H$_8$O$_7$·2H$_2$O, reagent grade, Wako Pure Chemical Industry Inc., Japan) were used to prepare the $La_{9.33+x}Si_6O_{26+1.5x}$ via a sol–gel process. La(NO$_3$)$_3$·6H$_2$O solution was first prepared by deionized water, in which the concentration of La^{3+} was determined by chelatometric titration method in advance. An appropriate amount of alcohol was added into the La^{3+} solution to prepare a solvent containing a volume fraction of 20% water. Subsequently, citric acid with the same molar as La(NO$_3$)$_3$·6H$_2$O and a stoichiometric amount of SiO$_2$ powder was added. A viscous gel was obtained by vigorous stirring at 80 °C. The dried LSO gel was then calcined at 800, 900 and 1000 °C for 3 h in air. The as-synthesized powders were ground and sieved. For 2/4-probe measurement, calcined LSO powders were pressed into disk/bar and isostatic cold-pressed uniaxially at 200 MPa, and then sintered at 1600 °C for 10 h in air. For 4-electrode configuration, two current electrodes covering two terminal surfaces of the bar sample and two voltage-reading electrodes in the form of two narrow strips spaced by 1 cm winding one circle of the bar were prepared by platinum paste.

Differential thermal analysis/thermo-gravimetric (DTA/TG, 6300, SII, Tokyo, Japan) and X-ray diffraction (XRD, M18XHF, Mac Science, Japan) were conducted to determine the phase formation and crystal structure of the calcined and sintered LSO. The LSO morphology was examined by transmission electron microscopy (TEM, JEM-2010F, JEOL, Tokyo, Japan) and scanning electron microscopy (SEM, JSM-7001F, JEOL, Japan). Electrical conductivities of the samples were carried out by 2 and 4-probe AC impedance measurements. The 4-probe measurements were approached based on an electrochemical interface (Impedance analyzer, 1287, Solartron, UK) in combination with an impedance analyzer (1260, Solartron, UK) over a frequency range of 0.01 Hz–8 MHz, in the temperature range of 200–800 °C in air.

3. Results and discussion

3.1. Morphological and structural analysis

Fig. 1 shows the thermal characteristics of the dried $La_{9.5}Si_6O_{26.25}$ gel. As observed in the DTA/TG curves, the strong exothermic peak around 200 °C associates with the combustion of citric acid, with a weight loss of 78.2%. The peak appears at 590 °C is attributed to the combustion of residual carbon. The crystallization of apatite from amorphous state occurs at 900 °C identified by a small exothermic peak in the DTA curve. No obvious thermal exchange reaction is identified in DTA/TG curves measured on cooling.

XRD profiles of the $La_{9.5}Si_6O_{26.25}$ calcined at various temperatures are shown in Fig. 2(a). The sample calcined at 800 °C exhibits

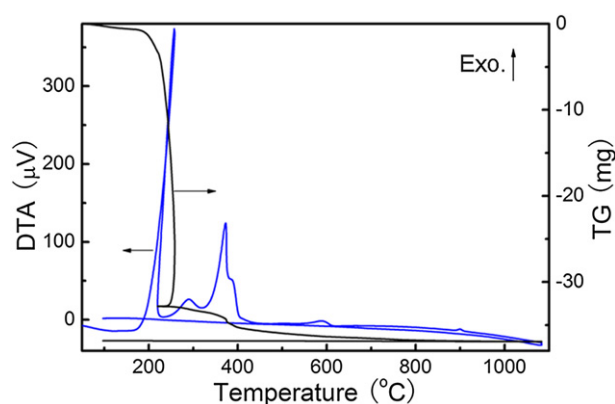Fig. 1. DTA/TG curves of dried LSO gel.

several broad peaks, indexed by the $La_2O_2CO_3$ peaks [4], which indicates that the formation of crystal LSO went through a mediate state of $La_2O_2CO_3$. The appearance of the $La_2O_2CO_3$ during calcination also can be verified by DTA result that the peaks between 300 and 400 °C in Fig. 1 is attributable to the dissociation of CO$_2$ from the $La_2O_2CO_3$. LSO sample calcined at 900 °C has rather pure apatite phase without any impurity trace, as well as benign crystallinity confirmed by more precise XRD pattern measured by step scanning technique shown in Fig. 2(b). In contrary, as shown in Fig. 2(a), corresponding to the peaks indicated by circles, secondary phase La_2O_3 occurs in LSO powders when increasing the calcination temperature to 1000 °C. Thus, the optimal calcination temperature is 900 °C for the formation of LSO powders with pure apatite-type phase.

The phase structure of LSOs sintered at 1600 °C has also been conducted by XRD, as shown in Fig. 3. It is noteworthy that the samples calcined at lower temperatures of 800 °C and 900 °C are pure oxy-apatite phase. While, high calcination temperature of 1000 °C leads to an impurity of La_2SiO_5 in the sintered LSO, which is the result of the reaction between the secondary phase La_2O_3 formed by decarburization reaction during calcination and silicate apatite in LSO powder during sintering process.

The TEM image in Fig. 4(a) illustrates the morphology of individual spherical nanoparticles in the LSO powder calcined at 900 °C, showing an average grain size of about 30 nm. The high resolution TEM (HRTEM) of the upper inset shows that the LSO powder is fine-grained with better crystallinity. The selected area electron diffraction (SAED) patterns shown in the lower inset is taken along [001]. The microstructure of thermally etched surfaces of LSO sintered body calcined at 900 °C followed by a sintering at 1600 °C is shown in Fig. 4(b). The relative density of the LSO body is 95.7% measured by an Archimedean method, which satisfies the application of solid electrolytes for SOFCs with a relative density of higher than 95%. Therefore, in our study the sintering temperature of LSO can be lowered to 1600 °C.

Furthermore, the composition dependence on the phase identified in LSO samples with various compositions is shown in Fig. 5. As the La content in the calcined and sintered LSOs increases, the secondary phase of La_2O_3 and La_2SiO_5 start to appear at the composition of $La_{10}Si_6O_{27}$ and $La_{9.50}Si_6O_{26.25}$, respectively. Fig. 6 depicts the Raman spectra of the sintered $La_{9.33+x}Si_6O_{26+1.5x}$, measured at room temperature, which show the presence of bands at 365–410 cm^{-1} and 525 cm^{-1}, attributed to the symmetric bending mode (v_2) and asymmetric bending mode (v_4) of the SiO$_4$ unit. The peak around 830–870 cm^{-1} is attributed to the symmetric stretching mode (v_1) and the weak peak at 980 cm^{-1} to the asymmetric stretching mode (v_3) [13–15]. The sintered LSO samples have pure apatite phase as 9.33 + x ≤ 9.5, while extra bands
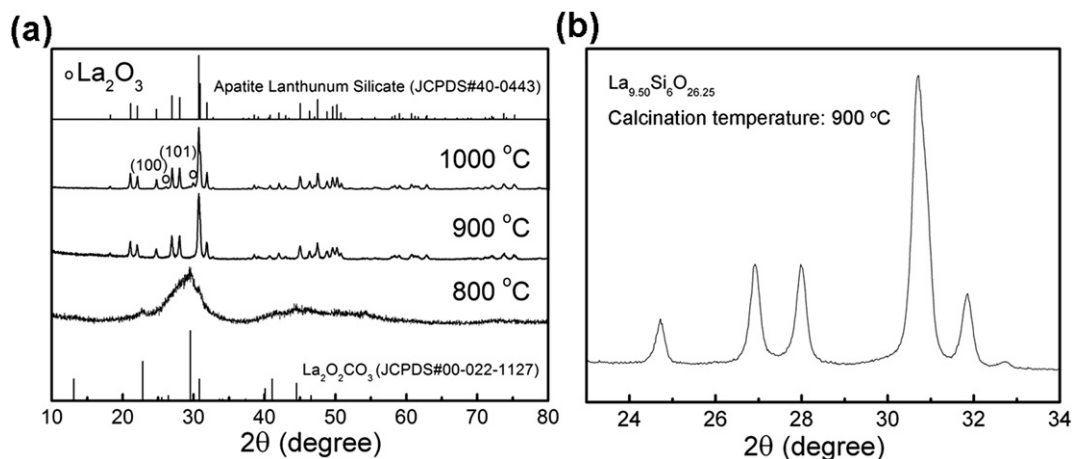
Fig. 2. (a) XRD patterns of the LSO powders calcined at various temperatures, together with (b) more precise XRD pattern measured by step scanning.
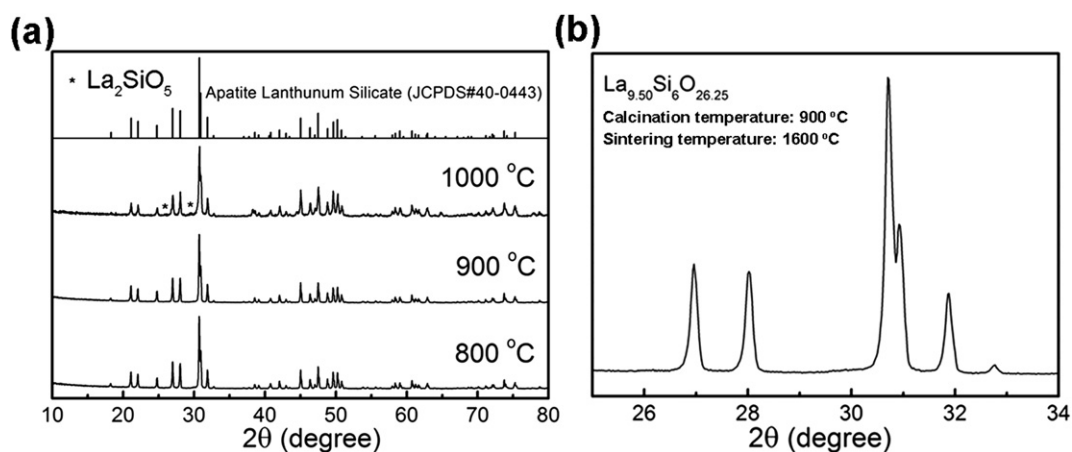

Fig. 3. (a) XRD patterns of the LSO samples calcined at various temperatures followed by a sintering at 1600 °C, together with (b) more precise XRD pattern measured by step scanning.

attributable to impurity phase of La_2SiO_5 appear in Raman spectra when $9.33 + x > 9.5$ [15]. The Raman analysis is soundly in agreement with the XRD results (Fig. 5(b)).

3.2. Electrical conductivity study

The electrical conductivities of the LSO electrolytes obtained from AC impedance spectra are substantially influenced by the electrode configuration on the samples. In our study, both 2 and 4-probe method are applied for the electrical conductivity measurement. The 4-probe method can eliminate the electrode polarization due to the current path and voltage-sensing electrodes are independent of each other. That is, typical AC impedance spectra collected by 4-probe measurement only exhibit semicircular arcs for the total resistance contribution including the grain and grain boundary, excluding the electrode component. The total resistance, therefore, can be obtained easily and clearly, as a result of the negligible influence of the interface/electrode on the impedance
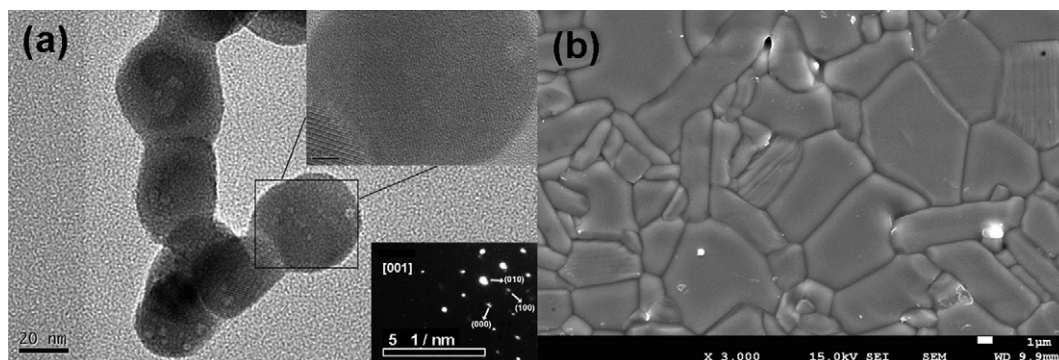

Fig. 4. (a) TEM image of the LSO powder. The upper inset is the HRTEM image and the lower one is the SAED pattern. (b) SEM images of the sintered LSO samples.
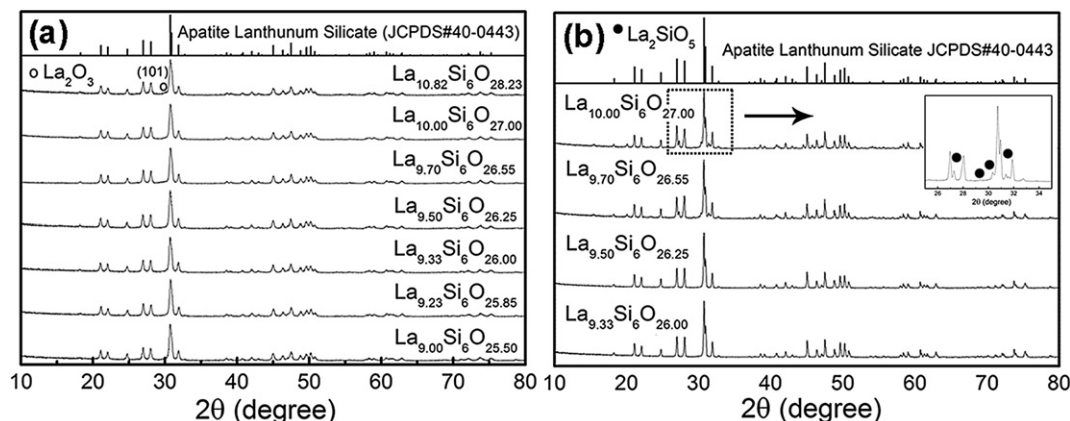
Fig. 5. (a) XRD patterns of the LSO powders and (b) sintered body with variety of compositions.
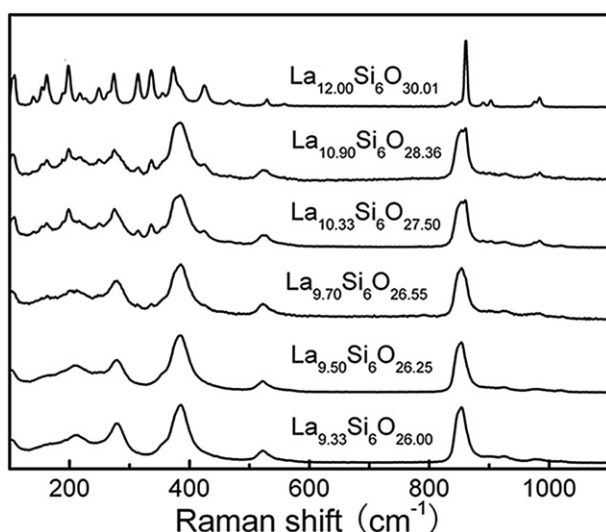

Fig. 6. Raman spectra of the LSO samples with variety of compositions.

spectra and the total resistance subsequently down to the low frequencies [16–19]. The impedance spectra of the $La_{9.50}Si_6O_{26.25}$ calcined at 900 °C and then sintered at 1600 °C by 4-probe method measured at various temperatures are shown in Fig. 7(a), which shows only one semicircular arc corresponding to the total

resistance and many measured points fall together into the same point on Z'-axis at low frequencies. The electrical conductivities of LSO are also measured by 2-probe method, which is equivalent to the results by 4-probe method.

In order to obtain the conductivity value, software of Z-view was applied to fit the impedance spectra. The total resistance is obtained as the resistance value at the intercept with the real axis. The electrical conductivity (σ) data for LSO can be converted from the resistance data R by the following equation:

$$\sigma = \frac{1}{R}\frac{L}{S},$$ (1)

where L and S are the thickness and the effective electrode area of the disk sample for the 2-probe method, respectively. On the other hand, for 4-probe impedance spectra, L corresponds to the distance between the voltage electrodes, and S is the area surface of two terminals of the bar sample.

The major carrier in LSO is of significant interest with regard to the potential use of this material as a solid electrolyte in SOFCs. Fig. 7(b) gives the electrical conductivity dependence on the oxygen partial pressure, which demonstrates that the conductivity does not change with pO_2, suggesting that the major carrier of LSO is oxide ion rather than electronic defects such as electrons and holes.

The temperature dependence of ionic conductivity for the LSO samples calcined at different temperatures and sintered at 1600 °C is depicted in Fig. 8(a), as an Arrhenius type plot, ln (σT) vs. 1000/T. It can be seen that the sintered LSO samples calcined at 900 °C
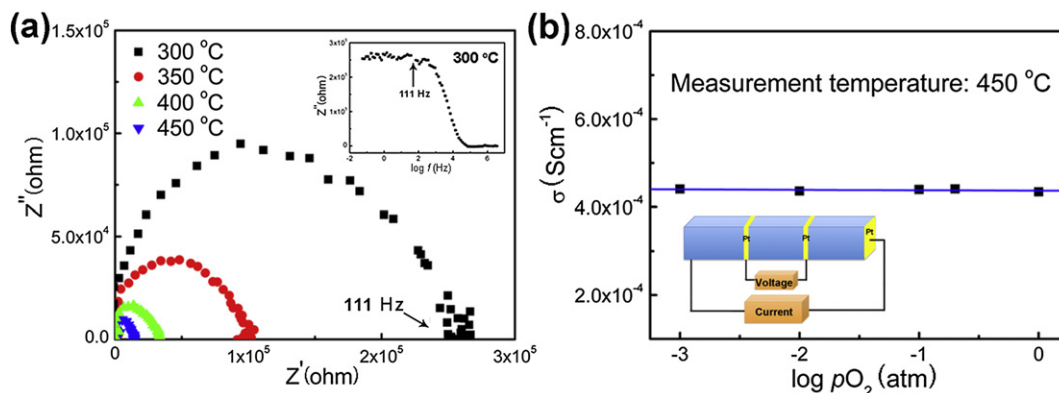

Fig. 7. (a) 4-probe impedance spectra of the LSO samples measured at various temperatures. The inset shows the Z″ vs log f curve at 300 °C. (b) Ionic conductivity of LSO as a function of the oxygen partial pressure measured at 450 °C. The inset shows the schematic illustration of the electrode configuration for 4-probe measurement.
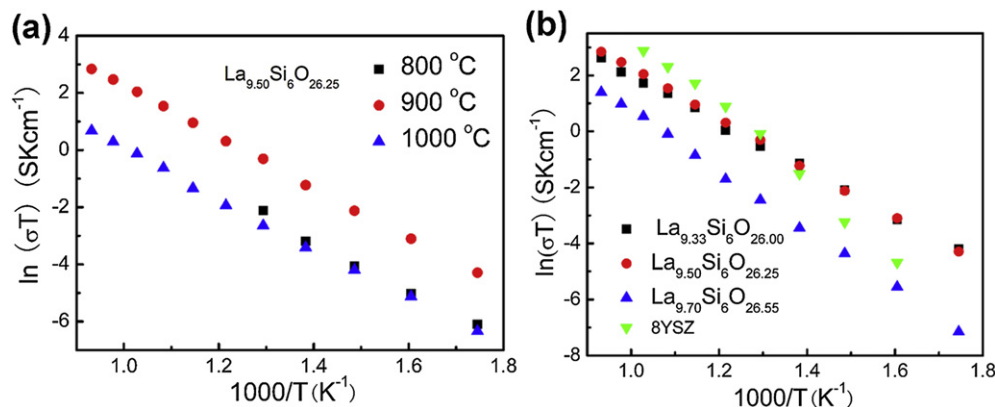
Fig. 8. Arrhenius plots of the LSO samples (a) with various calcination temperatures and (b) with various compositions.

exhibits the largest conductivity, which is due to the highest density. The relative densities of the sintered LSO samples calcined at various temperatures are measured by Archimedean method, showing that the samples calcined at 800 °C, 900 °C and 1000 °C have the relative densities of 91.4%, 95.7% and 84.6%.

Fig. 8(b) shows the Arrhenius plots of LSOs calcined at 900 °C and sintered at 1600 °C with various compositions, together with the data of 8YSZ, which indicates that LSOs ($La_{9.5}Si_6O_{26.25}$ and $La_{9.33}Si_6O_{26}$) has higher conductivity than 8YSZ in the intermediate/low temperature range, due to their lower activation energy in comparison to that of 8YSZ. It can be also seen from Fig. 8(b) that $La_{9.5}Si_6O_{26.25}$ has a little higher ionic conductivity than the sample with $La_{9.33}Si_6O_{26}$ composition. The conductivity of $La_{9.7}Si_6O_{26.55}$ is the lowest, probably due to the blocking of oxide ion migration by impurity phase in the sample. The ionic conductivities of $La_{9.5}Si_6O_{26.25}$ and $La_{9.33}Si_6O_{26}$ are 1.6×10^{-2} Scm^{-1} and 1.3×10^{-2} Scm^{-1} at 800 °C, respectively, which are much higher than reported values [8,20–23]. Higuchi et al. [20] have reported that the electrical conductivity of $La_{9.5}Si_6O_{26.25}$ at 800 °C is 8.0×10^{-3} Scm^{-1}. The conductivities of the $La_{9.33}Si_6O_{26}$ at 800 °C from Refs. [21,22] are 2.0×10^{-3} Scm^{-1} and 7.3×10^{-4} Scm^{-1}. Therefore, the sol–gel synthesis in our study yields high performance of the LSO electrolytes.

4. Conclusions

In conclusion, this work has demonstrated lanthanum silicates $La_{9.33+x}Si_6O_{26+1.5x}$ with a highly pure oxyapatite phase prepared by a sol–gel synthesis. The effect of calcination temperature on the phase stability, microstructure evolution and electrical conductivity of LSOs is investigated systematically by XRD, TEM, SEM and Raman. The calcined and sintered LSO samples with various compositions show pure apatite phase in the composition ranges of $9.33 + x \leq 9.5$ and $9.33 + x \leq 10$, respectively. The electrical conductivity of the LSO samples, measured and comparatively analyzed by 2 and 4-probe AC impedance spectroscopy, revealed

that the conductivities of $La_{9.5}Si_6O_{26.25}$ and $La_{9.33}Si_6O_{26}$ calcined at 900 °C and sintered at 1600 °C are 1.6×10^{-2} Scm^{-1} and 1.3×10^{-2} Scm^{-1} at 800 °C, which are higher than the LSO synthesized by a conventional method. Also the major carrier of LSO is confirmed to be of oxide ions.

References

[1] B.C.H. Steele, A. Heinzel, Nature 414 (2001) 345–352.
[2] B. Zhu, J. Power Sources 114 (2003) 1–9.
[3] A.C. Johnson, B.K. Lai, H. Xiong, S. Ramanathan, J. Power Sources 186 (2009) 252–260.
[4] K. Kobayashi, Y. Matsushita, N. Igawa, F. Izumi, C. Nishimura, S. Miyoshi, Y. Oyama, S. Yamaguchi, Solid State Ionics 179 (2008) 2209–2215.
[5] S. Nakayama, Y. Sadaoka, J. Mater. Chem. 3 (1993) 1251–1257.
[6] S. Nakayama, H. Aono, Y. Sadaoka, Chem. Lett. 6 (1995) 431–442.
[7] S. Nakayama, M. Sakamoto, J. Mater. Sci. Lett. 20 (2001) 1627–1629.
[8] Y. Kim, D.K. Shin, E.C. Shin, H.H. Seo, J.S. Lee, J. Mater. Chem. 21 (2011) 2940–2949.
[9] E. Béchade, I. Julien, T. Iwata, O. Massona, P. Thomasa, E. Championa, K. Fukuda, J. Eur. Ceram. Soc. 28 (2008) 2717–2724.
[10] A. Chesnaud, G. Dezanneau, C. Estournès, C. Bogicevic, F. Karolak, S. Geiger, G. Geneste, Solid State Ionics 179 (2008) 1929–1939.
[11] E. Kendrick, M.S. Islam, P.R. Slater, J. Mater. Chem. 17 (2007) 3104–3111.
[12] B. Li, W. Liu, W. Pan, J. Power Sources 195 (2010) 2196–2201.
[13] S.H. Jo, P. Muralidharan, D.K. Kim, Electrochim. Acta 54 (2009) 7495–7501.
[14] E. Rodríguez-Reyna, A.F. Fuentes, M. Maczka, J. Hanuz, K. Boulahya, U. Amadore, J. Solid State Chem. 179 (2006) 522–531.
[15] L. Zhang, H.Q. He, H.W. Wu, C.Z. Li, S.P. Jiang, Int. J. Hydrogen Energy 36 (2011) 6862–6874.
[16] C.H. Lee, H.B. Park, Y.M. Lee, R.D. Lee, Ind. Eng. Chem. Res. 44 (2005) 7617–7626.
[17] B.D. Cahan, J.S. Wainright, J. Electrochem. Soc. 140 (1993) L185–L186.
[18] J.R. Dygasa, G. Fafilekb, M.W. Breiterb, Solid State Ionics 119 (1999) 115–125.
[19] P. Kureka, G. Fafilek, Solid State Ionics 119 (1999) 151–158.
[20] Y. Higuchi, M. Sugawara, K. Onishi, M. Sakamoto, S. Nakayama, Ceram. Int. 36 (2010) 955–959.
[21] J.E.H. Sansom, P.R. Slater, Solid State Ionics 167 (2004) 23–27.
[22] S. Célérier, C. Laberty, F. Ansart, P. Lenormand, P. Stevens, Ceram. Int. 32 (2006) 271–276.
[23] S. Kikkawa, Y. Masubuchi, M. Higuchi, T. Takeda, J. Alloys Compd. 408–412 (2006) 641–644.